Università degli Studi di Trieste

Dipartimento di Ingegneria e Architettura
LM Ingegneria Meccanica

Numerical simulation of the flow in the ERCOFTAC diffuser

Termofluidodinamica Computazionale
Student project

Claudio Rossi *Mario Neri* *Giorgio Bianchi*

Academic Year 2022/2023

Contents

Abstract

In this report we describe the development and validation of a numerical model of the ERCOFTAC diffuser [1]. The simulation has been performed by means of the CFD package *Ansys® Fluent, Rel. 2022R1*, using a 2D, axisymmetric RANS model. It has been verified that the numerical results are free of convergence errors and are grid-independent. They are, on average, good or at least encouraging, and demonstrate the validity of the choices for the model that, while rather economical, provides a correct description of the physics of the problem.

1 Introduction

It is well known that in hydraulic power plants, downstream of the runner of Francis and Kaplan turbines (see figures 1 and 2), the water exits the turbine through a so-called *draft tube*, whose task is to act as a diffuser, i.e. to reduce the exit velocity with a minimum loss of energy. This decelerating flow induces a low static pressure just downstream the runner, with a consequent increase of the flow rate and output power of the turbine.

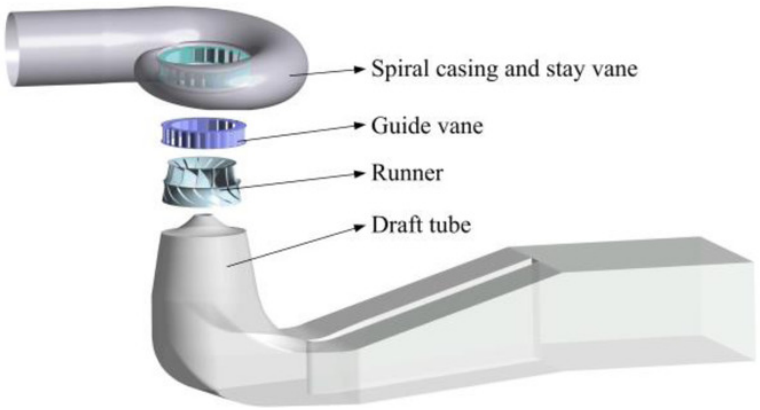

Figure 1: A Francis water turbine.

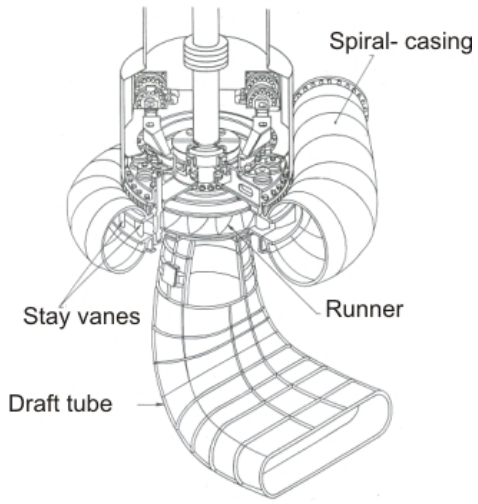

Figure 2: A Kaplan water turbine.

The draft tube can be considered as an axial-conical diffuser or in other words an axisymmetric expansion of a circular pipe. Its purpose is to improve the efficiency of the hydraulic turbine, converting a significant part of the kinetic energy of the fluid into static pressure. This is possible due to the streamwise increase of the cross-sectional area of the draft tube.

In this work we have numerically investigated the flow inside the ERCOFTAC diffuser [1] by means of the CFD package *Ansys® Fluent, Rel. 2022R1.*

This problem, although simplified, presents many of the characteristic features of the diffusers found in most Kaplan and Francis turbines, and therefore it represents an excellent *benchmark* for the validation of CFD models and procedures.

It is found that the numerical results agree reasonably well with the available experimental measurements.

2 Description of the problem

In this report, as already indicated, we have investigated the flow inside the ERCOFTAC conical diffuser described in [1]. The experimental measurements have been taken by Clausen et al. [2], and they are available, in a convenient tabular form, in [1]. In their measurements, the authors have investigated, in great detail, the *swirling turbulent boundary layer*. For this problem, in fact, the flow is characterized by the presence of *swirl*, as it is commonly found in the diffusers of real turbines when they operate at partial load. It is known that moderate levels of *swirl* delay the detachment of the boundary layer and thus they favor pressure recovery and increase the overall efficiency of the diffuser. However, excessive levels of *swirl* may induce recirculating regions within the diffuser which in turn lead to a reduction of efficiency of the device.
Previous CFD calculations for this problem have been conducted, among others, by Armfield et al. [3], From et al. [4] and by Bounous [5].

2.1 Experimental setup

The experimental setup used by Clausen et al. [2] is depicted in figure 3, where it can be noted that the ERCOFTAC diffuser, which has a length of 510 mm and an angle of 20°, is located downstream a *swirl* generator. The *swirl* is obtained by rotating a *honeycomb screen*, located at 500 mm upwind of the diffuser, and its containing wall whose length is equal to 400 mm. All other parts of the system are locked. The diffuser discharges at atmospheric pressure.

During the experimental tests, the air velocity at the inlet was set $U_0 = 11.6$ m/s, while the rotating wall and the screen had a rotating velocity of $\omega = 52.646$ rad/s. With this setup, the authors [2], claim that no recirculation zones were detected inside the diffuser.

2.2 Available measurements

The measurements, as illustrated in figure 4, have been taken along eight different cross sections, all perpendicular to the wall, one upstream of the diffuser inlet at $x = -25$ mm, and seven along the diffuser at $x = 25, 60, 100, 175, 250, 330, 405$ mm, where x is the local coordinate along the wall of the diffuser.

The following measurements were taken:

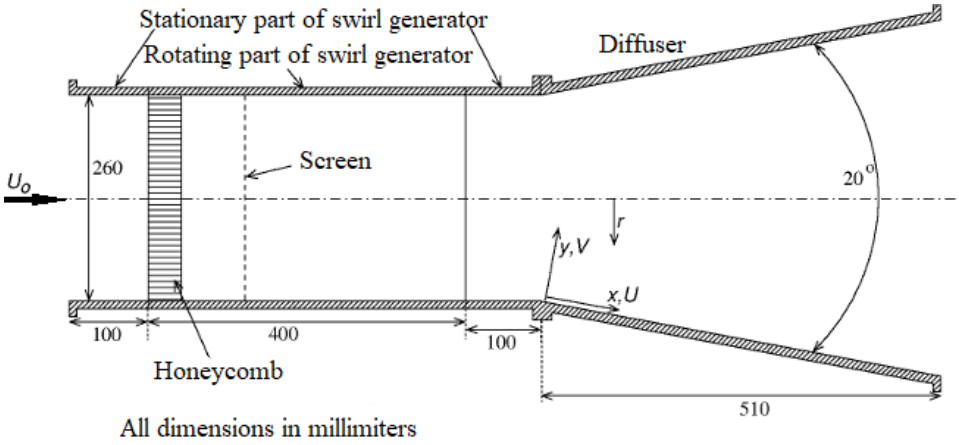

Figure 3: Experimental setup for the ERCOFTAC diffuser [1].

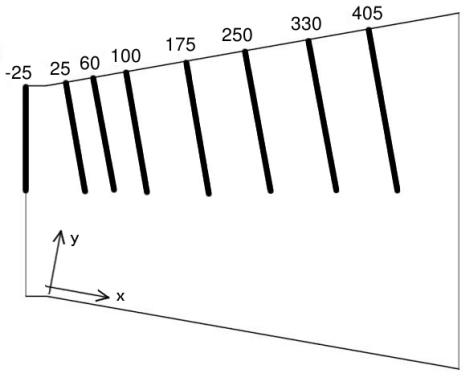

Figure 4: Measurement cross-sections for the ERCOFTAC diffuser [1].

- Static pressure measurements were obtained using wall taps. The pressure coefficient is defined as

$$C_p = \frac{p}{\frac{1}{2}\rho U_0^2} \tag{1}$$

- Profiles of axial velocity U and circumferential velocity W at the eight locations.
- Profiles of all six Reynolds stresses $\overline{u'^2}$, $\overline{v'^2}$, $\overline{w'^2}$, $\overline{u'v'}$, $\overline{u'w'}$, $\overline{v'w'}$ at the eight cross sections.
- Values of the wall shear stresses τ_{wx}/U_0^2 and τ_{wz}/U_o^2, and values of the wall shear angle $\beta_w = \tan^{-1}(W/U)_{y=0}$ at the above eight locations.

2.3 Flow parameters

The main *flow parameters* of the test-case are summarized here:

- Air with a kinematic viscosity $\nu = 1.5 \times 10^{-5}$ m^2/s.
- Average axial velocity at inlet: $U_0 = 11.6$ m/s.
- Reynolds number: $Re_D = \frac{U_0\, D}{\nu} = 202,000$.
- Atmospheric pressure at outlet.

3 Numerical method

3.1 Model equations and assumptions

The problem is tackled using a steady *RANS* (Reynolds Averaged Navier Stokes) approach, i.e. all flow variables are time-averaged (filtered) assuming an infinite time interval, thus obtaining steady-state RANS equations.

Turbulence is modeled using the *Realizable* $k-\varepsilon$ two-equations eddy viscosity turbulence model, using the *Enhanced Wall Treatment* with *pressure gradient effects*. The choice of this turbulence model is motivated by the fact the it provides improved predictions for flows involving rotation and boundary layers under strong adverse pressure gradients, like in this problem. Some preliminary calculations using other turbulence models, like i.e. the *Shear Stress Transport* (SST) model [7] and a full *Reynolds Stress* (RSM) model [8], did not provide any substantial improvement and, in addition, exhibited higher computational costs or, for the RSM, some difficulties in convergence.

Since the flow is considered steady and incompressible, a two-dimensional axisymmetric domain, with swirl, is assumed. This has been set in ANSYS Fluent by selecting, under *Physics* → *General*, *Pressure-based, Steady* solver, and *Axisymmetric Swirl* as 2D Space.

For the numerical algorithm, the following choices have been made:

- *Coupled* pressure-velocity coupling method.
- *Least-square* method for gradient reconstruction.
- *Second order upwind* scheme for all transported variables, including the turbulent quantities.
- *Warped-face* gradient correction.

3.2 Computational domain

The 2D axisymmetric computational domain is depicted in figure 5, while its dimensions are summarized in table 1.

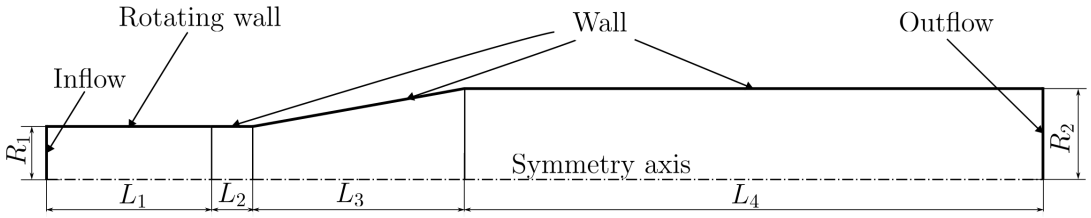

Figure 5: Computational domain.

R_1	R_2	L_1	L_2	L_3	L_4
130	220	400	100	510	1400

Table 1: Domain dimensions in mm.

From figure 5 one notes that in the numerical model, differently than the experimental setup, a long cylindrical pipe has been added downstream the diffuser, in order to minimize

the effects of the outflow boundary conditions in the flow field [5]. Furthermore, although the honeycomb was not directly modelled, its effects have been taken in due consideration by appropriate boundary conditions (see section 3.3).

3.3 Boundary conditions

To better reproduce the experimental setup, the following boundary conditions have been set. At the inlet it was assumed a velocity profile with a constant axial component $U_0 = 11.6$ m/s, a tangential component $U_\theta = \omega \cdot r$, and a radial component $U_r = 0$, where $\omega = 52.646$ rad/s is the angular velocity and r is the radial distance from the axis. The turbulence at the inlet has been specified, following Armfield et al. [3] and Bounous [5], with the *Intensity and Length Scale* option, in order to better replicate the experimental conditions, assuming a turbulence intensity of 4 %, and a Turbulent Length Scale of 0.0032 m.
At the walls a *no-slip* condition was assumed, and the rotating part of the wall was set as a moving wall with an absolute rotational speed of $\omega = 52.646$ rad/s. No boundary condition was necessary on the axis. At the outflow a *pressure-outlet* with a gauge pressure of 0 Pa was assumed. For convenience the boundary conditions are summarized in table (2).

Location	Boundary condition(s)	Value(s)	Comment
Inlet	Axial velocity U_x	11.6 [m/s]	From measurements
	Radial velocity U_r	0.0 [m/s]	From measurements
	Swirl angular velocity ω	52.646 [rad/s]	Swirl
	Turbulence intensity	4 [%]	From measurements
	Turbulence length scale	0.0032 [m]	From measurements
Fixed wall	Velocity components	0.0 [m/s]	No-slip
Rotating wall	Speed ω	52.646 [rad/s]	Measured
Outlet	Gauge pressure	0 [Pa]	Pressure-outlet

Table 2: Boundary conditions.

3.4 Grid generation

Given the simple geometry of the problem, we have decided to adopt block-structured quad-only grids. The blocking, illustrated in figure 6, and the corresponding grids, have been realized using ANSYS Mesh, using *Face Meshing* as the mesh generation method.

Figure 6: Subdivision in blocks of the computational domain.

Several grids have been realized, and their main characteristics are listed in table 3. The value of the *vertical bias* was imposed as *Bias Factor* when setting *Edge Sizing* along the

vertical lines of the blocks, in order to increase the resolution of the grid towards the walls. Its value was gradually decreased, when the resolution of the grid increased, in order to maintain a value of y^+ which does not vary significantly from one mesh to the next.

Grid	No. of cells	Vertical bias
A	5100	80
B	10000	70
C	21600	60
D	44100	50
E	75600	40
F	114000	35
G	196000	30

Table 3: Main characteristics of the grids.

Figure 7 depicts, as an example, grid B and its detail close to the initial part of the diffuser.

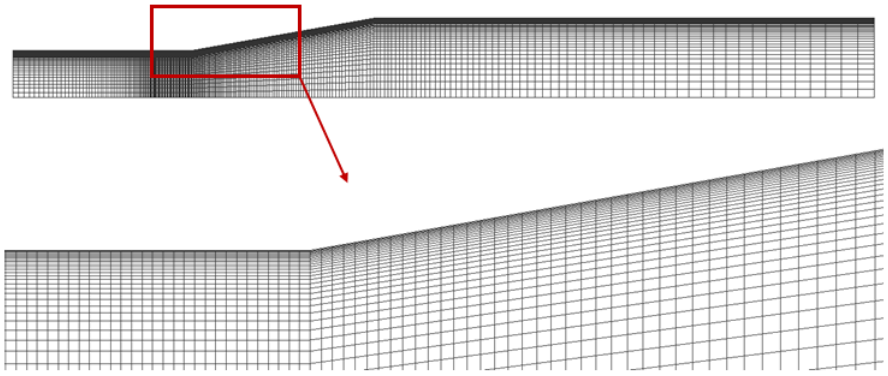

Figure 7: View of mesh B of table 3 and a detail close to the wall of the diffuser.

4 Preliminary calculations

To perform the analysis of the problem, several preliminary calculations have been performed in advance, in order to guarantee that convergence error are almost absent, and that the results are, as much as possible, grid-independent. For this purpose, two monitor variables have been defined in ANSYS Fluent, and their values have been recorded during the iterations:

1. Pressure difference $\Delta P = P_2 - P_1$ between the average pressure at two sections of the diffuser: P_1 at $x = 0.3$ m and P_2 at $x = 1.51$ m, respectively.

2. Velocity V_{mon} at a specific point: $x = 0.75$ m and $y = 0.1$ m.

The pressure planes and the velocity point are depicted in figure 8.

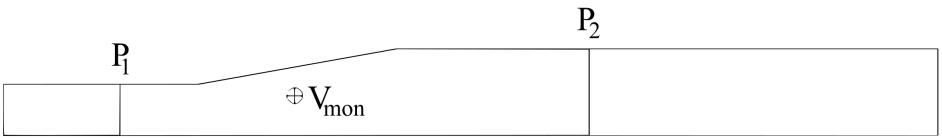

Figure 8: Pressure planes and velocity point used to monitor convergence.

4.1 Convergence error

In order to evaluate the value of residuals that guarantees an almost negligible convergence error, it has been decided to perform this evaluation on *grid D*, a medium-size grid, of table 3. The results are reported in table 4.

Residual	ΔP [Pa]	V_{mon} [m/s]
1×10^{-3}	71.85	7.403
1×10^{-4}	71.86	7.403
1×10^{-5}	71.86	7.403
1×10^{-6}	71.86	7.403

Table 4: Convergence on grid D of table 3

It can be observed, in table 4, that the monitored variable ΔP and V_{mon} do not change beyond a residual value of 1×10^{-4}. However, for conservative reasons, it has been decided to adopt a residual of 1×10^{-5} in the following analysis.

4.2 Grid independence

The same monitored variable, ΔP and V_{mon}, have been used to identify the minimum level of grid resolution which guarantees a *grid-independent solution*.
Table 5 reports the value of the monitor variable for the grids of table 3 for a residual of 1×10^{-5}. On the same table, for completeness, also the values of y^+, on the fixed and rotating wall, are listed.

Grid	ΔP [Pa]	V_{mon} [m/s]	y^+ fixed wall	y^+ rotat. wall
A	72.09	7.60	4.19	5.11
B	72.00	7.55	3.52	4.29
C	71.91	7.46	2.67	3.22
D	71.86	7.40	2.06	2.47
E	71.85	7.39	1.84	2.20
F	71.85	7.38	1.63	1.95
G	71.84	7.37	1.37	1.64

Table 5: Values of monitored variables and y^+ for the different grids.

To better appreciate the trend, the same data for ΔP and V_{mon} are graphically shown in figure 9.

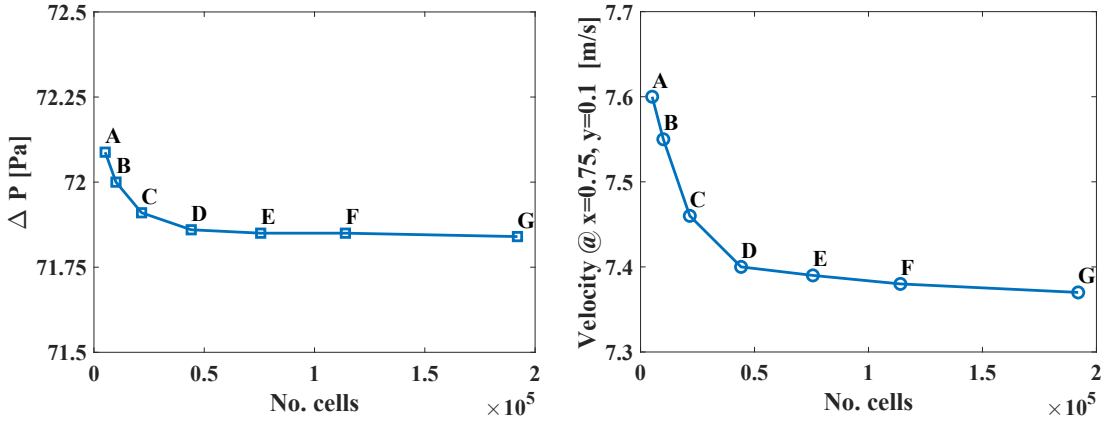

Figure 9: Values of the monitor variables with different grid resolution: (a) ΔP; (b) V_{mon}.

From figure 9 it can be noticed that, beyond grid D, both monitored variables ΔP and V_{mon} are almost unaffected by further increase of grid resolution. For this reason, all the following results have been collected on grid D.

5 Results

5.1 Quantitative results

The comparison between measured and computed values of C_p (see eqn. (1)) is given in figure 10. The agreement between measurements and CFD results is quite good at the

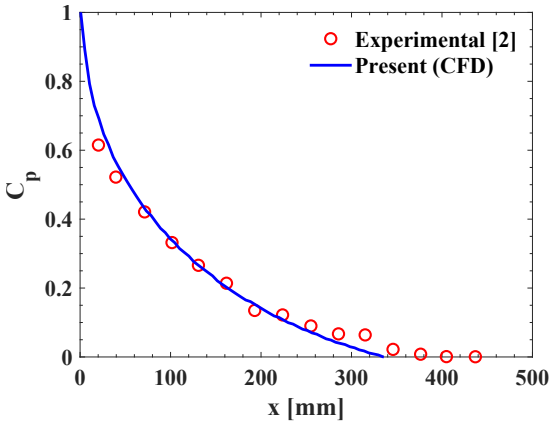

Figure 10: Pressure coefficient C_p on the diffuser wall.

beginning of the diffuser, but then it deteriorates further downstream. This means that our model is only partially able to reproduce the pressure recovery in the diffuser.
The comparison between measured and CFD predictions for the axial velocity at some of the cross-sections of figure 4 is displayed in figure 11.

From figure 11 it results an overall good agreement between experiments and simulation, in particular at the first cross-sections, while the agreement decrease moving further downstream, as already seen for the pressure coefficient. Regarding other quantities, a comparison between experimental and numerical data for the swirl velocity W and turbulent kinetic energy k are reported in figures 12 and 13, respectively.

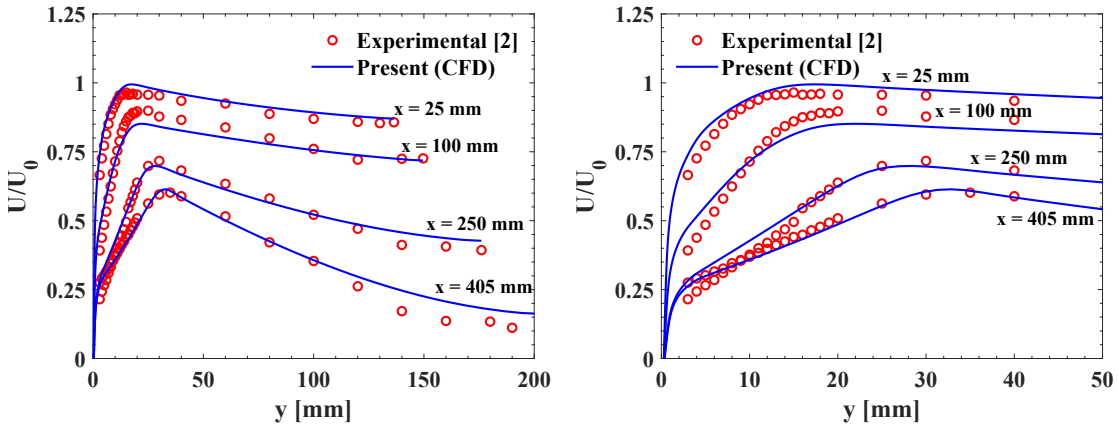

Figure 11: Axial velocity at different cross-sections: (a) overall; (b) close to the wall.

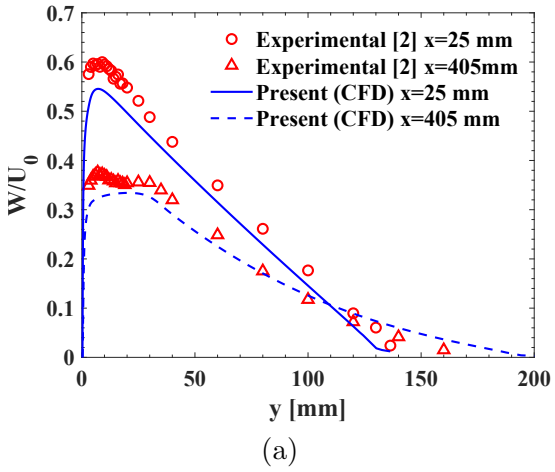

Figure 12: Swirl velocity.

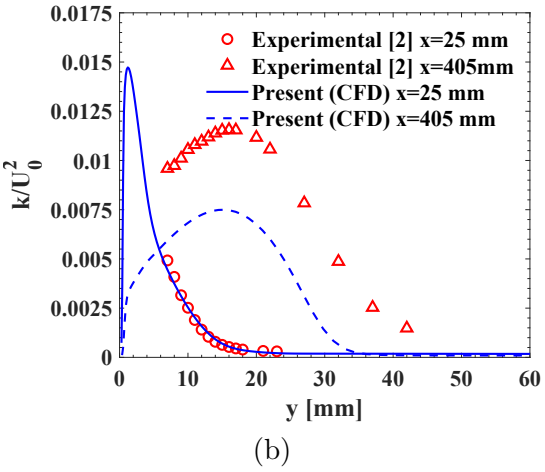

Figure 13: Turbulent kinetic energy.

While the comparison between measurements and CFD results for the swirl velocity W is satisfactory, this is not the case for the turbulent kinetic energy k: the agreement is rather good for the first cross-section at $x = 25$mm, but at $x = 405$ mm only the qualitative trend is similar, but in quantitative terms the difference between experiments and simulation is high, of the order of 40%.
This disagreement might explain the previous differences between measured and computed velocity profiles along the last cross-sections of the diffuser.

5.2 Flow pattern

In the following, we show some visualizations that can help to understand the flow pattern for this problem.
The pressure field is given in figure 14, where the pressure recovery provided by the diffuser is clearly visible.

The flow pattern is well described by the streamlines reported in figure 15. It can be noted that, in our simulation, a small recirculation bubble is present immediately downstream the conical part of the diffuser. However, at present, is hard to claim if this is a feature of the flow field in the diffuser or is just a numerical artifact: in the experiments

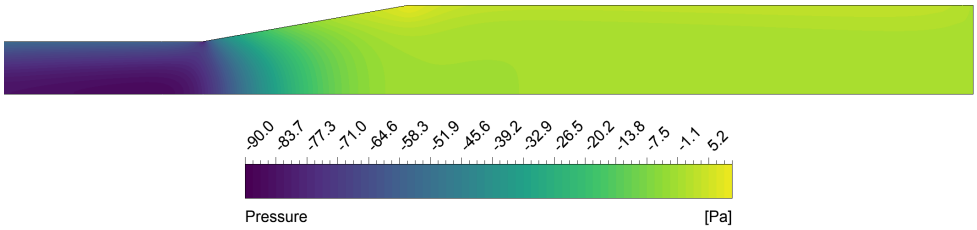

Figure 14: Pressure field in the diffuser.

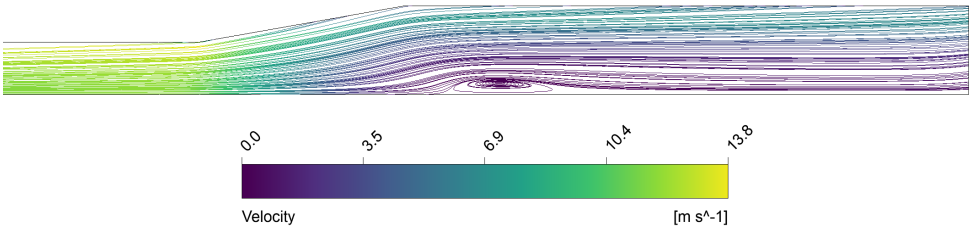

Figure 15: Streamlines in the diffuser.

there was no evidence of recirculation, although the measurements were taken only *within* the diffuser and not downstream. In any case, we have to keep in mind that the intensity of this recirculation is very weak, as evidenced by the vector plot of the velocity field in figure 16, where it can bee seen that most of the flow is concentrated toward the walls.

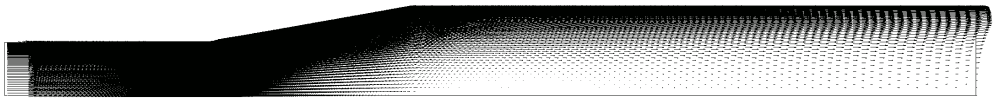

Figure 16: Velocity vector plot in the diffuser.

6 Concluding remarks

In this project we have described our methodology and the corresponding results for the numerical simulation of the ERCOFTAC diffuser [1] by means of the CFD package *Ansys® Fluent, Rel. 2022R1*. From the results obtained, the following conclusions can be drawn:

- The adoption of a computationally inexpensive 2D axisymmetric steady model allowed us to reach a grid-independent solution, free of convergence errors. Thus, any difference between measurements and calculations can be entirely attributed to modeling errors like *i.e.* choice of the domain, boundary conditions, turbulence model *et.*

- Although the system and its associated geometry was overly simplified - e.g. the filter was not modeled *et.* - the proper choice of boundary conditions that could replicate the real system was quite effective, since the agreement between experimental data and simulation results can be generally considered good or at least encouraging.

- The discrepancy between experiments and numerical data is rather low in the first part of the diffuser, but increases further downstream, as proved by the poor prediction of the turbulent kinetic energy profile at the last cross-section of the diffuser.

- Some calculations performed using different turbulence models, like i.e. the *SST* (Shear Stress Transport) model, and even a full differential *RSM* (Reynolds Stress) model, did not show any substantial improvement, proving that, for the *RSM* model, probably the anisotropy of the Reynolds Stresses was not a major cause of discrepancy between measurements and calculations.

- From the previous consideration it follows that, in order to improve the quality of the prediction, it is unclear if the choice of other RANS turbulence models, with specific adjustments and tuning (see [4]), would be very beneficial, or if a a complete different modeling, *e.g.* a scale-resolving approach like *LES* (Large Eddy Simulation), *DES* (Detached Eddy Simulation), *DDES* (Delayed Detached Eddy Simulation), *SAS* (Scale Adaptive Simulation) *et.*, would be the best choice, keeping however in mind the conspicuous increase in computational resources required by these models.

References

[1] http://cfd.mace.manchester.ac.uk/ercoftac/doku.php?id=cases:case060

[2] D. Clausen P., G. Koh S., and H. Wood D. Measurements of a swirling turbulent boundary layer developing in a conical diffuser, *Experimental Thermal and Fluid Science*, **6**, pp. 39-48, 1993. https://doi.org/10.1016/0894-1777(93)90039-L

[3] S.W. Armfield, N.-H. Cho and C.A.J. Fletcher, *AIAA Journal*, **28**, No. 3, pp. 453-460, 1990.

[4] C.S. From, E. Sauret, S.W. Armfield, S.C. Saha, Y.T. Gu, Turbulent dense gas flow characteristics in swirling conical diffuser, *Computers and Fluids*, **149**, pp. 100-118, 2017. https://doi.org/10.1016/j.compfluid.2017.03.021

[5] O. Bounous, Studies of the ERCOFTAC Conical Diffuser with OpenFOAM, *Research report 2008:05*, Dept. Appl. Mechanics, Chalmers University of Technology, Göteborg, SWEDEN, 2008.

[6] T.-H. Shih, W. W. Liou, A. Shabbir, Z. Yang, and J. Zhu, A New k- ε Eddy-Viscosity Model for High Reynolds Number Turbulent Flows - Model Development and Validation, *Computers Fluids*, **24(3)**:227-238, 1995. https://doi.org/10.1016/0045-7930(94)00032-T

[7] F.R. Menter, Two-Equation Eddy-Viscosity Turbulence Models for Engineering Applications, *AIAA Journal*, **32**, no. 8, 1994.

[8] B. E. Launder, G. J. Reece and W. Rodi, Progress in the development of a Reynolds-stress turbulence closure, *J. Fluid Mechanics*, **68 (3)**, 537–566, 1975. https://doi:10.1017/s0022112075001814